Atmos. Chem. Phys. Discuss., 12, 15977–16024, 2012
www.atmos-chem-phys-discuss.net/12/15977/2012/
doi:10.5194/acpd-12-15977-2012

Atmospheric Chemistry and Physics Discussions

Formaldehyde and nitrogen dioxide over the remote Western Pacific Ocean: SCIAMACHY and GOME-2 validation

E. Peters[1], F. Wittrock[1], K. Großmann[2], U. Frieß[2], A. Richter[1], and J. P. Burrows[1]

[1]Institute of Environmental Physics (IUP), University of Bremen, Otto-Hahn-Allee 1, 28359 Bremen, Germany
[2]Institute of Environmental Physics (IUP), University of Heidelberg, Im Neuenheimer Feld 229, 69120 Heidelberg, Germany

Received: 4 June 2012 – Accepted: 7 June 2012 – Published: 28 June 2012

Correspondence to: E. Peters (enno.peters@iup.physik.uni-bremen.de)

Published by Copernicus Publications on behalf of the European Geosciences Union.

Abstract

In October 2009, ship-borne Multi-Axis Differential Optical Absorption Spectroscopy (MAX-DOAS) measurements were performed during the TransBrom campaign over the Western Pacific Ocean (≈40° N to −20° S). Vertical tropospheric trace gas columns and profiles of nitrogen dioxide (NO_2) and formaldehyde (HCHO) as well as stratospheric NO_2 columns were retrieved in order to validate corresponding measurements from the GOME-2 and SCIAMACHY satellite instruments and to estimate tropospheric background concentrations of these trace gases.

All instruments reproduced the same characteristic latitude-dependent shape of stratospheric NO_2. SCIAMACHY and GOME-2 data differ by about 1 % from each other while yielding lower vertical columns than MAX-DOAS morning values as a consequence of measurement time and stratospheric NO_2 diurnal cycle. At low latitudes, an increase of $8.7 \pm 0.5 \times 10^{13}$ molec cm^{-2} h^{-1} of stratospheric NO_2 was estimated from MAX-DOAS data.

Tropospheric NO_2 was above the detection limit only in regions of higher anthropogenic impact (ship traffic, transport of pollution from land). A background column of 1.3×10^{14} molec cm^{-2} (or roughly 50 ppt BL concentration) can be estimated as upper limit for the remote ocean, which is in agreement with GOME-2 monthly mean values. In the marine boundary layer close to the islands of Hokkaido and Honshu, up to 0.8 ppbv were retrieved close to the surface.

Background HCHO concentrations over the remote ocean exhibit a diurnal cycle with maximum values (depending strongly on weather conditions) of 4×10^{15} molec cm^{-2} for the vertical column at noon-time. Corresponding peak concentrations of up to 1.1 ppbv were retrieved in altitudes of 400–600 m around noon while maximum concentrations in the evening are close to the ground. An agreement between MAX-DOAS and GOME-2 data was found for typical vertical columns of 3×10^{15} molec cm^{-2} over the remote ocean at the time of overpass.

ACPD
12, 15977–16024, 2012

1 Introduction

Nitrogen dioxide (NO_2) and formaldehyde (HCHO) are important trace gases in the atmosphere. They can be detected by remote sensing techniques due to their characteristic absorption features in the Visible and the UV spectral range, respectively.

The nitrogen oxides NO and NO_2 ($NO + NO_2 = NO_x$) are prominent pollutants in the troposphere, harmful for lung tissue, powerful oxidants and key ingredients in the formation of tropospheric ozone. They are produced predominantly at high temperatures in combustion processes, both anthropogenic (burning of fossil fuel in industry and traffic) and biogenic (bush and forest fires), as well as in soil microbial processes and lightning events (Lee et al., 1997). As a consequence, NO_2 is detected above industrialized and urban areas, traffic routes and over bush fires (e.g. Richter and Burrows, 2002; Richter et al., 2004; Franke et al., 2009; Konovalov et al., 2010). In higher concentrations, NO_2 can be observed even by eye as it causes the typical brownish color of polluted air and exhaust plumes. Sinks for NO_2 are the reaction with the hydroxyl radical OH and photolysis. The former reaction produces nitrous acid (HNO_3) leading to acidification of precipitation and therefore of soil and water. Photolysis of NO_2 produces ozone and NO, which can react again with ozone to form NO_2. Thus, in the absence of peroxide radicals (e.g. in a remote, clean environment) an equilibrium between NO, NO_2 and ozone would develop as a function of sunlight intensity.

In the stratosphere, the nitrogen oxides NO and NO_2 are key ingredients in catalytic cycles leading to ozone depletion (Crutzen, 1970; Johnston, 1971). They are transported upwards in form of the long lived nitrous oxide (N_2O) originating from anthropogenic sources (e.g. traffic) and microbiological activity in soil (Bates and Hays, 1967). Reaction of N_2O with excited oxygen atoms in the stratosphere, produced mainly by UV photolysis of ozone, yields then nitrogen monoxide (Brasseur et al., 1999), which is subsequently converted to NO_2.

Formaldehyde (HCHO) is the simplest and most abundant aldehyde in the atmosphere belonging to the huge family of oxygenated volatile organic compounds

ACPD
12, 15977–16024, 2012

(OVOCs). It is produced during photochemical degradation of methane (CH_4) and non-methane hydrocarbons (NMHC). The oxidation of methane produces a global HCHO background with reported surface levels of 0.2–1 ppbv in remote marine environments (Weller et al., 2000; Singh et al., 2001; Burkert et al., 2001). In addition, HCHO originates from biomass burning and fossil fuel combustion (Anderson et al., 1996) and vegetation (Seco et al., 2006). The major sinks of HCHO are photolysis at wavelengths below 400 nm, reaction with OH and wet deposition, resulting in a short lifetime of a few hours (Arlander et al., 1995). As a consequence, elevated HCHO levels are found close to its sources, over rainforests, bush fires or shipping routes (e.g. Marbach et al., 2009; Stavrakou et al., 2009).

NO_2 and HCHO have been observed from space for many years (e.g. Richter et al., 2005; Leue et al., 2001; Martin et al., 2002; Wittrock et al., 2000; Palmer et al., 2003; De Smedt et al., 2008) by means of the well-known DOAS technique (Platt, 1994) fitting trace gas absorption features to recorded spectra of backscattered sunlight from Earth. Satellite instruments provide a global image of NO_2, HCHO and other trace gas distributions and allow to detect and observe source regions of high concentrations (e.g. Richter et al., 2004, 2005; Wittrock et al., 2006; Marbach et al., 2009; Stavrakou et al., 2009). Nevertheless, these instruments have problems to detect trace gases over remote oceanic regions as concentrations in the troposphere are usually low there. Thus, the accuracy of these measurements is unclear. In addition, the low albedo of the ocean's surface as well as spectral structures introduced by liquid water absorption and vibrational Raman scattering in water leaving radiance limits the accuracy of satellite measurements (Vountas et al., 2003). On the other hand, independent remote sensing ground based measurements to validate satellite measurements of NO_2 and HCHO in marine regions are rare as they have been performed predominantly over land (e.g. Wittrock et al., 2006; Irie et al., 2008) and so far ship-borne MAX-DOAS measurements have been focused on other trace gases (e.g. Martin et al., 2009; Sinreich et al., 2010) or were not aiming at validating satellite measurements (e.g. Takashima et al., 2011).

ACPD
12, 15977–16024, 2012

Objectives of this study are to (i) estimate background columns of tropospheric HCHO and NO_2 in a remote marine environment as well as stratospheric NO_2 columns and their latitudinal distribution and (ii) validate satellite measurements of the SCIAMACHY and GOME-2 instruments with independent ground-based MAX-DOAS measurements. These measurements were performed during the TransBrom cruise in October 2009 (Krüger and Quack, 2012) in the Western Pacific region. A MAX-DOAS instrument uses a similar measurement technique as satellite DOAS-instruments, but due to the viewing geometry, a much longer light path in the lower troposphere can be achieved. Therefore a MAX-DOAS instrument is more sensitive for tropospheric absorbers and allows estimating tropospheric trace gas columns and concentrations in a remote environment with better accuracy. Thus, it is applicable for the validation of satellite instruments.

2 The TransBrom campaign

The TransBrom campaign was carried out onboard the German research vessel *Sonne* departing from Tomakomai, Japan (42°38′ N, 141°37′ E) on 9 October 2009 and arriving in Townsville, Australia (19°15′ S, 146°49′ E) on 24 October 2009. The campaign's main objective was to measure bromine compounds in the ocean water and their flux into the atmosphere. The Western Pacific region is considered to be the main entrance gate into the stratosphere where the bromine originating from ocean water could contribute to ozone depletion (Quack, 2010).

One focus of the participation of the IUP Bremen research team and MAX-DOAS instrument was the study of atmospheric bromine monoxide (BrO), which is not the topic of this manuscript. Here, we focus on trace gas columns of NO_2 and HCHO, which were derived simultaneously from the performed MAX-DOAS measurements, in order to validate the space-borne SCIAMACHY and GOME-2 measurements.

The cruise track is shown in Fig. 1a together with 72 h backward trajectories calculated with the online model HYSPLIT (Draxler and Rolph, 2011; Rolph, 2011) from

ACPD
12, 15977–16024, 2012

the National Oceanic and Atmospheric Administration (NOAA) indicating prevailing westerly wind directions throughout the whole campaign. Therefore, except for the beginning of the campaign having been influenced from near Japanese islands, the measurements yield typical results for background levels in the remote oceanic troposphere.

The extratropical storm *Melor* hit Japan shortly before the campaign and our MAX-DOAS instrument could therefore only be set up at sea when wind gusts ceased. 10 October was dominated by good viewing conditions and almost clear sky, 11 and 12 October were increasingly cloudy. A second storm *Nepartak* with wind speeds of $20\,m\,s^{-1}$ forced a course correction in the night from 12 to 13 October. From morning to noon of 13 October, it was raining heavily before the ship encountered best viewing conditions and almost clear sky on 14 October. 15–19 October were partly cloudy and occasionally it was raining. Apart from the beginning of the cruise, 19 October was the only event when 72 h backward trajectories reached to mainland (here: the island of New Ireland). 20 to 22 October were dominated by an almost full cloud coverage and occasional heavy rains, before the viewing conditions improved again towards the end of the cruise. As the backward trajectories in Fig. 1a indicate, strong winds from the open sea were prevailing from 20–24 October (during the whole cruise across the Coral sea).

Figure 1b shows all measurement pixels from the GOME-2 satellite instrument taken within a 200 km radius around the ship's position at the time of the overflight (≈09:30 LT). For 13, 14 and 21 October, no satellite pixels were available at the corresponding ship's location.

In Fig. 1c, ship positions reported to the US Coast Guard's Automated Mutual-Assistance Vessel Rescue System (AMVER) for the duration of 9–24 October 2009 are displayed, giving an impression of the ship density and preferred shipping routes (Doug Horton, US Coast Guard Operations Systems Center, personal communication, 2010). After leaving the polluted region around Japan, the cruise encountered a clean oceanic environment with very limited anthropogenic activities. Red arrows in Fig. 1c

ACPD
12, 15977–16024, 2012

indicate locations where tropospheric NO_2 events were observed in the MAX-DOAS data (Fig. 6).

3 Instruments and data analysis

3.1 The (MAX-)DOAS measurement principle

For the retrieval of NO_2 and HCHO, the well established Differential Optical Absorption Spectroscopy (DOAS) technique is used (Platt and Stutz, 2008). The DOAS method is a remote sensing technique using scattered sunlight spectra and is based on the attenuation of light traveling through the atmosphere according to the Lambert-Beer law. The basic idea is to separate the optical thickness (logarithm of the ratio of a measured spectrum to a reference spectrum, which usually is a direct solar spectrum for satellite retrievals and a spectrum in zenith viewing direction for ground-based instruments) in a high frequency component describing absorption processes by trace gas molecules, and a low frequency component accounting for scattering and instrumental effects. Trace gas cross-sections from laboratory measurements are fitted together with a polynomial accounting for the low frequency components to the optical thickness yielding so called (differential) slant column densities (which are often called slant columns (SC), for simplicity) as fit parameters. These have units of molecules per area and represent the respective trace gas concentration integrated over the light path. For ground-based instruments, the retrieved slant columns are not absolute, but the difference between the slant column of the respective measurement and the slant column of the reference measurement. Consequently, to obtain absolute slant columns, the reference slant column has to be known (e.g. from complementary measurements) or estimated (e.g. Langley plot, look-up climatology).

Sensitivity for trace gases at different altitudes depends on the measurement geometry, which is used by ground-based Multi-AXis (MAX)-DOAS measurements (Hönninger et al., 2004; Wittrock et al., 2004). Tropospheric absorbers are measured at elevation

ACPD
12, 15977–16024, 2012

angles close to the horizon (the elevation angle is defined as the angle between the horizon and the viewing direction) as the resulting light path in the troposphere is longer then, whereas the sensitivity for stratospheric absorbers is high in zenith viewing direction during twilight due to a long light path through the stratosphere under these conditions.

To convert the obtained slant columns to vertical columns (VC), which represent the respective trace gas concentration integrated over altitude, radiation transport models are used to calculate so called airmass factors (AMF), the ratio between slant columns and vertical columns (see Sect. 3.5).

3.2 Satellite instruments

The Scanning Imaging Absorption spectroMeter for Atmospheric CHartography (SCIAMACHY) instrument is a UV-Vis-NIR spectrometer on board the ESA satellite ENVISAT launched into a sun-synchronous, near-polar orbit in March 2002 measuring backscattered radiation from the Earth's atmosphere or surface (Burrows et al., 1995; Bovensmann et al., 1999). The instrument consists of 8 simultaneously measuring channels, six continuous channels from 214–1750 nm and two further channels for near-infrared light. The equator crossing time is 10:00 LT, the spatial resolution depends on species and illumination and is typically $60 \times 30\,km^2$ for the data used here. Full coverage at the equator is achieved every six days.

The Global Ozone Monitoring Experiment-2 (GOME-2) instrument is derived from SCIAMACHY and the GOME instrument, which flew on ERS-2 from 1995 to 2011 (Burrows et al., 1999, and references therein). It is a UV/Vis nadir-viewing grating spectrometer on board the MetopA satellite that was launched into a sun synchronous orbit in October 2006 (Callies et al., 2000). The instrument measures solar radiation scattered and reflected by the atmosphere and covers a wavelength region from 240–790 nm with a spectral resolution of 0.2–0.4 nm. The equator crossing time is 09:30 LT, the nominal ground-pixel size $40 \times 80\,km^2$ ($240 \times 40\,km^2$ for the back scan). Near global coverage is achieved due to a large scan width of 1920 km every day.

ACPD
12, 15977–16024, 2012

3.3 Ground-based instrumentation and set up on the ship

The IUP Bremen MAX-DOAS instrument comprises a telescope unit, which is connected via a split optical fiber bundle with two spectrometers. The telescope unit is mounted on a commercial ENEO VPT-501 Pan-Tilt-Head, which allows pointing it in any viewing direction. Light is entering the telescope through a fused silica window to avoid cut-off of UV radiation and is focused by a lens on the optical fiber bundle entrance. The telescope's field of view (FOV) is ≈1.2° but may be slightly increased due to the pointing accuracy at sea (see Sect. 3.4). The fiber bundle consists of 76 single fibers and has a length of 20 m. After that it splits into two fiber bundles consisting of 38 single fibers each, leading to two spectrometers, one for UV and one for the visible spectral range. The fiber bundle arrangement allows separating the light collecting telescope unit from the spectrometers and also overcomes polarization effects. The spectrometers are actively temperature stabilized at 35 °C. The UV spectrometer (ANDOR Shamrock 303i, 1200 l mm^{-1} grating) is equipped with a two-dimensional ANDOR Newton DU940N CCD camera with 512 × 2048 pixels. It covers the spectral range of 315–384 nm with an average resolution (FWHM of the slit function) of 0.4 nm. The Vis spectrometer is an Acton500 with a two dimensional ROPER CCD camera with 100 × 1340 pixels covering a wavelength interval from 400–570 nm at a resolution of 0.8 nm.

In addition to the lens-fiber system, the telescope unit contains a video camera for scene documentation and a Mercury/Cadmium (HgCd) line lamp for calibration measurements. Snapshots from the video stream were taken every 5 s during the whole campaign, giving the possibility to identify events in the trace gas measurement time series (e.g. passing of other ships) as well as viewing condition surveillance (e.g. cloud cover, rain). All measurements and system operations are controlled by an in-house software.

ACPD
12, 15977–16024, 2012

The excellent instrument's performance has been demonstrated in the intercomparison campaign CINDI a few months before TransBrom (Roscoe et al., 2010; Piters et al., 2012; Pinardi et al., 2012), where it was selected as one of the reference instruments.

During the cruise, the telescope unit was mounted at the monkey deck above the bridge of the RV Sonne pointing portside (Fig. 2), which was the western direction for most of the cruise (compare to Fig. 1a). Vertical scans were performed in viewing directions orthogonal to the ship's movement in 1° steps from −3° to 6° and additionally at 8°, 10°, 15° and 30° elevation angles. At the end of each scanning sequence, a zenith spectrum (used as reference spectrum in the DOAS retrieval) was recorded. In off-axis directions (all viewing angles except zenith) the integrated measurement time for each direction was 40 s consisting of several individual measurements of 100 ms each. In zenith direction an integration time of 120 s was applied.

3.4 Data processing and filtering

As the ship is pitching and tossing in the sea, the elevation angles of the telescope (which are relative to the ship) are not the actual viewing directions. To overcome this effect, spectra were recorded with exposure times of 100 ms. The ship's movements were considered to be negligible within this period. In addition, the ship's heading, pitch and roll angle were recorded every 50 ms and downloaded from the ship's data base at the end of the cruise. For each vertical scanning sequence, the single 100 ms measurements were then corrected in terms of the roll angle and sorted according to the real viewing direction with a tolerance of ±0.5°. These corrected individual measurements were then averaged for each viewing angle. As a result, the precision of the viewing direction is ±0.5°, but the time resolution is reduced to the duration of one scanning sequence (typically 10–15 min).

In addition, the wind direction was recorded from the ship's weather surveillance systems. To avoid contamination from the ship's exhaust plume, those individual measurements taken under *bad* wind directions (relative wind directions between 80° and 270° with respect to the bow, see Fig. 2) were removed before averaging.

ACPD
12, 15977–16024, 2012

3.5 Data analysis

For the NO_2 retrieval, a fitting window from 450–497 nm was applied according to (Richter, 1997). Absorption cross-sections of ozone at 223 K (Bogumil et al., 2003), NO_2 (Vandaele et al., 1996), the oxygen dimer O_4 (Hermans et al., unpublished, http://spectrolab.aeronomie.be/o2.htm), water vapor (HITRAN database, http://www.cfa.harvard.edu/hitran/) as well as a calculated pseudo-cross section accounting for Rotational Raman Scattering (RRS) on air molecules known as the Ring effect (Vountas et al., 1998), a 3rd order polynomial and an additive offset were considered in the fit.

For the HCHO retrieval, following the analysis described in (Heckel et al., 2005) detecting tropospheric HCHO with a ground-based MAX-DOAS instrument and the recommendations given in (Pinardi et al., 2012), a fitting window from 335–357 nm was applied. Cross-sections of ozone at 223 K and 273 K, NO_2, O_4 (see references above), HCHO at 297 K (Meller and Moortgat, 2000), BrO (Fleischmann et al., 2004) as well as a pseudo-cross section accounting for the Ring effect, a 4th order polynomial and an offset were fitted to the recorded optical depths to retrieve slant columns.[1]

As an example, Fig. 3 shows a tropospheric NO_2 DOAS fit (top) and a HCHO fit (bottom).

Stratospheric vertical columns for NO_2 were obtained by dividing the slant columns by airmass factors calculated with the radiative transfer model (RTM) SCIATRAN (Rozanov et al., 2005), version 2.2 during twilight from 88° to 92° solar zenith angle

[1]For the analysis of iodine monoxide (417–439 nm) above the ocean (Großmann et al., 2012), an improvement was achieved by applying a pseudo cross-section accounting for inelastic scattering on molecules in liquid water (Vibrational Raman Scattering, VRS) in the DOAS fit. Its calculation and application in other wavelength regions including the NO_2 fitting window used in this study is subject of current investigation. In the UV, this effect is expected to affect the DOAS fit to a lesser extent as the relative number of photons travelling through liquid water before being scattered in the telescope is lower (as the absorption coefficient of liquid water increases in the UV, see e.g. Raymond and Baker, 1981).

ACPD
12, 15977–16024, 2012

(SZA). As input parameters for the radiative transfer model, pressure, temperature and trace gas profiles from the US standard atmosphere were used.

The retrieval of tropospheric vertical columns and/or trace gas profiles from obtained slant columns in different elevation angles is an inverse problem. One method to solve this is the well-known optimal estimation method (Rodgers, 2000). Here, all NO_2 and HCHO tropospheric columns were retrieved using the BRemian Advanced MAX-DOAS Retrieval Algorithm (BREAM) (Wittrock, 2006). BREAM uses a two-step approach. As the light path and therefore the slant columns especially in viewing directions close to the horizon depend strongly on the aerosol load, first, an aerosol extinction profile is estimated from comparing measured slant columns of the oxygen dimer (O_4) with O_4 slant columns that were simulated with the RTM SCIATRAN for different aerosol extinctions. In this step also a correlation factor between measured and simulated O_4 slant columns is calculated to detect cloudy scenes that cannot be corrected for by the applied aerosol extinction profile and the corresponding measurements are removed. In the second step, again using the RTM SCIATRAN, block airmass factors are calculated for the weighting functions describing the relation between the measured slant columns in different elevation angles and the vertical trace gas profile of interest. Then the optimal estimation is performed using an appropriate a priori trace gas profile. The retrieval grid consists of 80 equally spaced layers of 50 m each (total height 0–4 km). Retrieval studies under different scenarios have shown that this profiling algorithm is capable of reproducing the trace gas column within an error of 20 % and the volume mixing ratio (VMR) in the lowest 500 m within 25 %; for these studies and more information on the principles of MAX-DOAS profile algorithms see (Wittrock et al., 2012; Wittrock, 2006).

Similar profiling techniques based on the optimal estimation method have been used recently, e.g. to retrieve BrO profiles and aerosols in the Arctic (Frieß et al., 2011). HCHO and NO_2 vertical distributions have been retrieved in the polluted region of Milano, Italy, using parametrization techniques for block-profiles (Wagner et al., 2011) expecting the trace gases in the boundary layer (or an uplifted layer). In contrast, the

ACPD
12, 15977–16024, 2012

troposphere over the remote ocean is considered to be very clean and no sources of HCHO and NO_2 are located at the surface (except for the sparse events of other ships passing). The background concentrations are assumed to originate from methane oxidation and lightning events, respectively, and therefore they are not strictly linked to the boundary layer. Thus, no block-profiles but volume mixing ratios decreasing linearly with altitude were used as a priori profiles in the optimal estimation.

The information content of the profile retrieval depends on the actual viewing conditions. Here, typical values for the number of degrees of freedom are 2 to 3.

For the SCIAMACHY satellite retrieval of NO_2, a fitting window from 425–450 nm was applied. For the stratosphere, only the stratospheric AMF was used and no correction for clouds or the troposphere has been taken into account. For the troposphere, only pixels with <0.2 cloud coverage were considered (FRESCO+) (Wang et al., 2008) and a tropospheric AMF based on a MOZART NO_2 profile climatology was used. A reference sector (longitude 180°–210°) was subtracted to correct for the stratospheric NO_2 content. The applied DOAS fit settings are explained in detail elsewhere (Richter et al., 2005).

For the GOME-2 retrieval of NO_2 the same settings were used, but an extended fitting window from 425–497 nm was applied (Richter et al., 2011).

For the HCHO retrieval from GOME-2 a fitting window from 337–353 nm was applied (Vrekoussis et al., 2010).

4 Results

4.1 Stratospheric NO_2

In the stratosphere, NO_2 undergoes a diurnal cycle due to photolysis of N_2O_5 (causing NO_2 to increase during the course of the day, e.g. a recent study found an increase of 6×10^{13} molec cm^{-2} h^{-1} for the subtropics, Gil et al., 2008). The N_2O_5 is build up at night from the reaction of NO_2 with O_3 and subsequent reactions (Brasseur et al., 1999). As

ACPD
12, 15977–16024, 2012

a result of this diurnal cycle, the content of NO_2 in the reference measurement cannot be obtained using a simple Langley plot, as it requires constant conditions during the day. Therefore, a fixed reference measurement was used for the whole campaign taken on 14 October a.m. (latitude 20.5° N), as this was the period with best weather and viewing conditions and the region is representative for open ocean conditions with negligible tropospheric NO_2 content (see Sect. 4.2 and Fig. 6). The SCIAMACHY and GOME-2 (interpolated) data imply a vertical column of about 1.9×10^{15} molec cm^{-2} for this day at their overflight times (10:00 LT and 09:30 LT, respectively) when the MAX-DOAS performed measurements at 40° SZA. Consequently, the slant column of this reference measurement was estimated to be

$$SC_{ref} = AMF \cdot VC_{ref} \approx \frac{1.9 \times 10^{15}}{\cos(40)} \approx 2.5 \times 10^{15} \text{ molec cm}^{-2}$$

This reference SC was added to daily twilight measurements taken between 88° and 92° SZA and calculated airmass factors (Sect. 3.5) were used to obtain vertical columns that were averaged for a.m. and p.m., respectively. An uncertainty of 30 % of the reference vertical column would correspond to $\approx 0.7 \times 10^{15}$ molec cm^{-2} in the reference slant column, which is added to the twilight measurements. With an airmass factor of ≈18 for measurements taken at 90° SZA this would lead to an uncertainty of 0.04×10^{15} molec cm^{-2}, which is negligible (compared to values in Fig. 4). The tropospheric NO_2 column across the ocean is even lower than 0.7×10^{15} molec cm^{-2} (see Sect. 4.2) and has therefore been neglected.

In Fig. 4 the resulting stratospheric NO_2 vertical columns from MAX-DOAS are displayed in magenta (a.m. values) and blue (p.m. values) as a function of latitude (see also Fig. 1 for the cruise track). GOME-2 and SCIAMACHY satellite data is displayed in green and red, respectively. GOME-2 satellite pixels were averaged within a 200 km radius around the ship's position at the overflight time (for the location of GOME-2 satellite pixels being averaged, see Fig. 1b). For the SCIAMACHY instrument, averages within a 400 km radius were calculated to account for its parser spatial coverage.

ACPD
12, 15977–16024, 2012

Both, the MAX-DOAS a.m. and p.m. values as well as the satellite values show a characteristic U-shape with latitude. MAX-DOAS a.m. values range from 2.3×10^{15} molec cm^{-2} at 35° N to 1.3×10^{15} molec cm^{-2} across the Equator and increase to 1.8×10^{15} molec cm^{-2} at 13° S (note that especially at the beginning of the cruise values are missing due to instrumental problems and data with *bad* wind directions that were removed). MAX-DOAS p.m. values slowly decrease from 3.8×10^{15} molec cm^{-2} at 38° N to 2.5×10^{15} molec cm^{-2} at the equator and increase again to 3.8×10^{15} molec cm^{-2} at 19° S. This general shape is in good agreement with results from a previous campaign performed in the Atlantic ocean (Kreher et al., 1995) while absolute values seem to be slightly smaller.

Figure 5 shows exemplarily the diurnal cycle derived from MAX-DOAS measurements on 15 October 2009 (latitude 16.4° N). For this figure, AMFs have been calculated not only for measurements between 88° and 92° SZA, being most sensitive to stratospheric absorbers due to the long light path in the stratosphere, but for all measurements. The sensitivity decreases rapidly for small SZAs since the light path through the stratosphere diminishes. Consequently, the variance in retrieved NO_2 columns (grey data points in Fig. 5) increases. In order to increase the number of measurements yielding better statistics, all viewing directions >5° elevation angle were considered to contain only stratospheric NO_2 signals. This is a reasonable assumption as 15 October 2009 had open ocean conditions with negligible tropospheric NO_2 content (see Sect. 4.2 and Fig. 6). The resulting vertical columns (grey data points in Fig. 5) have been binned to 0.5 h steps (blue data points). After the a.m. value (indicated by a dashed line), the stratospheric NO_2 columns decrease towards a minimum and increase afterwards, reproducing the a.m. value around noon. A linear regression between 07:00 LT and 16:00 LT yields a slope of $(8.7 \pm 0.5) \times 10^{13}$ molec cm^{-2} h^{-1}. Consequently, the satellite values in Fig. 4 should be $\approx 1.7 \times 10^{14}$ molec cm^{-2} lower than MAX-DOAS a.m. values due to their overflight time, which is slightly more than observed but in agreement with most of the observations considering the error bars (see Fig. 4). At the beginning of the campaign, on 10 and 11 October 2009 (latitudes 38.7°

ACPD
12, 15977–16024, 2012

and 34.1° N), the satellite pixels considered for the comparison include areas over or close to Japan (Fig. 1b), a region of high anthropogenic pollution, meaning that polluted pixels may affect the satellite averages.

For the whole dataset shown in Fig. 4, SCIAMACHY and GOME-2 agree with each other within their standard deviations resulting from spatial averaging (error bars of satellite data). The mean difference between the satellite instruments for this analysis is $(0.17 \pm 1.00) \times 10^{14}$ molec cm^{-2} (corresponding to 0.7–1.1 % of the vertical column). While reproducing the same latitudinal shape as the MAX-DOAS data, SCIAMACHY is on average $(0.26 \pm 1.04) \times 10^{14}$ molec cm^{-2} and GOME-2 $(0.53 \pm 1.30) \times 10^{14}$ molec cm^{-2} lower than the MAX-DOAS a.m. values, as a consequence of the stratospheric NO_2 diurnal cycle as discussed above.

4.2 Tropospheric NO_2

At low latitudes, the large concentration of water vapor in the humid air above the warm ocean's surface potentially limits the accuracy of the MAX-DOAS measurements as small misfits of H_2O would dominate the DOAS fit residual. This has been seen under similar conditions by (Takashima et al., 2011) where it is discussed in detail. Here we could avoid this problem by using the Hitran 2009 update for the water vapor cross section (HITRAN database, http://www.cfa.harvard.edu/hitran/) and the fitting window between 450 and 497 nm.

Figure 6 shows all retrieved NO_2 slant columns throughout the whole cruise that were taken under wind directions preventing the ship's exhaust plume to contaminate the measurements (see Sect. 3.4). In addition, suspicious high and short-in-time peaks, especially when showing larger slant columns in high elevation angles, were removed as being most probably due to wind gusts blowing the plume into the instrument's line of sight (the distance between the instrument and the exhaust plume was only a few meters). As the MAX-DOAS measurements from the southward moving ship will contain a contribution from stratospheric NO_2 which shows a latitudinal variation (see

ACPD
12, 15977–16024, 2012

Sect. 4.1), for each measurement the closest zenith[2] measurement was chosen as reference to minimize the stratospheric NO_2 signal. For comparison, Fig. 7 shows the monthly mean tropospheric NO_2 vertical columns as observed from the space-borne GOME-2 instrument.

The elevation angle in Fig. 6 is color coded, smaller elevations yielding higher slant columns as the light path through the trace gas layer is longer (this information is used for the profiling retrieval). After the first days of the cruise, having influences from Japan (Figs. 1 and 7), no split-up of different viewing directions is observed and elevated tropospheric NO_2 columns in the clean air over the open ocean were detected only for three events (arrows in Fig. 6) corresponding to the position of the ship indicated by red arrows in Fig. 1c. Also on 10 and 11 October, being in the polluted marine environment close to Japan, peaks were found in the dataset. For all events, lower elevation angles show enhanced NO_2 slant columns while the NO_2 at 30° elevation angle is not (or only slightly) enhanced. This behaviour indicates that the observed NO_2 is close to the ground and not originating from our ship's plume as this would increase the 30° elevation angle more than elevation angles close to the horizon. The spikes on 11 and 20 October are short-in-time and affect only measurements within single scans. These events could be assigned to other ship plumes as the video camera in our telescope housing detected other ships passing exactly at the time of these peaks. In comparison to these high and short-time events, elevated levels of NO_2 on 22 October are lower but persist for a time span of ≈3 h. The video camera did not detect any other vessels for this event, but Fig. 1c indicates the crossing of a clearly preferred shipping route. Higher concentrations of NO_2 along frequently used shipping routes is a known issue having been observed from space-borne platforms (e.g. Beirle et al., 2004; Richter et al.,

[2]Note that for 11 October almost no zenith measurements exist due to instrumental problems and the 30° elevation was chosen as reference which will strongly reduce the sensitivity towards NO_2 in the free troposphere; nevertheless, it turned out that the NO_2 is close to the surface (Fig. 9) giving the possibility to achieve reasonable results even using the 30° reference for NO_2 measurements.

ACPD
12, 15977–16024, 2012

2004). The origin of the events on 10 October remaining for ≈1 h is unclear. Backward trajectories calculated with the online tool HYSPLIT (Draxler and Rolph, 2011; Rolph, 2011) from the National Oceanic and Atmospheric Administration (NOAA) reach back to the Japanese mainland on 10 October, so that influences from the close Japanese coast (i.e. passing of towns, industrial regions) can be an explanation. The event in the evening of 19 October consists of multiple scans with increasing NO_2 slant columns, a clear maximum of 12×10^{15} molec cm^{-2} and a rapid decrease afterwards. Emissions from other vessels missed by our telescope camera are a possible explanation. In addition, this event coincides with elevated levels of formaldehyde in the evening of 19 October when a minimum distance of ≈150 km is reached to the Island of New Ireland and calculated backward trajectories reach back to the island suggesting also transport events (see discussion in Sect. 4.3).

For the first days of the cruise (10–11 October 2009) the profiling software *BREAM* (see Sect. 3.5) was used to calculate NO_2 vertical columns (Fig. 8) and profiles (Fig. 9). As Fig. 9 shows, maximum NO_2 concentrations are observed close to the ground. Apart from the peaks as discussed above (yielding up to 0.8 ppbv peak concentrations), the background concentrations do not exceed 0.2 ppbv even in the polluted marine environment close to Japan.

For the tropospheric NO_2 column and concentration above the open ocean, where NO_2 slant columns were close to the detection limit (Fig. 6), an upper limit has been estimated. Best RMS of the tropospheric NO_2-Fits are $\approx 1 \times 10^{-4}$ and the differential NO_2 absorption cross-section is in the order of 1×10^{-19} cm^2 molec^{-1}. Assuming that an optical density of twice the RMS can be detected, a limit of 2×10^{15} molec cm^{-2} for the slant column can be estimated. This corresponds to a vertical column of $\approx 1.3 \times 10^{14}$ molec cm^{-2} with a typical airmass factor of 15 for low elevation angles. Under the assumption of a block-profile of 1 km mixing layer height (MLH), this vertical column (VC) yields a volume mixing ratio (VMR) of

$$\mathrm{VMR} = \frac{\mathrm{VC}}{\mathrm{MLH}} \cdot \frac{k_\mathrm{B} \cdot T}{p} \approx 50\,\mathrm{pptv}$$

ACPD
12, 15977–16024, 2012

with the Boltzmann constant k_B, $T = 300\,K$ and $p = 1 \times 10^5\,Pa$. This detection limit can be regarded as an upper limit for the tropospheric NO_2 column under clean open ocean conditions, which is less than reported by (Takashima et al., 2011) who found 0.2 ppbv as an upper limit for the marine background concentration of NO_2 in the lowest 1000 m.

Tropospheric vertical columns derived from GOME-2 and SCIAMACHY satellite measurements are shown in Fig. 8 as color coded data points in comparison to the MAX-DOAS values. For this comparison, all satellite pixels within a 150 km radius around the ship's position at the time of the overflight were averaged for GOME-2 (for SCIAMACHY, 200 km averages have been calculated to account for the poorer spatial coverage). As a consequence of the spatial averaging, pixels over or close to Japan may increase the satellite averages, as there is a strong gradient in NO_2 pollution from land to ocean (see Fig. 7). This results also in the large standard deviations displayed as satellite error bars in Fig. 8. As a result, the satellite averages are 2–3 times higher than corresponding MAX-DOAS measurements, but agree within their standard deviations. For comparison, also the MAX-DOAS vertical columns from measurements within 200 km distance from the ship's geolocation at the satellite overpass have been averaged[3] and are displayed as brown data points in Fig. 8.

For the open ocean, satellite vertical columns from GOME-2 monthly average are $<2 \times 10^{14}\,molec\,cm^{-2}$ (Fig. 7), which is below the estimated uncertainty of the satellite (Boersma et al., 2004), but in good agreement with the background vertical column of $1.3 \times 10^{14}\,molec\,cm^{-2}$ derived from MAX-DOAS data.

4.3 Tropospheric HCHO

Source regions of formaldehyde (rain forests emitting precursors and direct anthropogenic emissions from industry) can be identified from space as Fig. 11 illustrates. The cruise track indicated in Fig. 11 implies that the MAX-DOAS formaldehyde

[3] And were plotted at their average measurement time. As the satellite overpass is before noon, the MAX-DOAS averages are plotted at later times.

ACPD
12, 15977–16024, 2012

measurements performed during TransBrom are far away from these source regions giving therefore the opportunity to investigate the formaldehyde background concentration originating from methane oxidation and evaluating the accuracy of satellite measurements of small formaldehyde columns over the ocean.

In contrast to NO_2, no formaldehyde is expected to be in the stratosphere and therefore no stratospheric contribution has to be accounted for (i.e. by using the closest zenith spectrum as a reference). For the formaldehyde DOAS-fit, a daily reference spectrum at 45° SZA was used as the fit quality turned out to decrease using zenith measurements at small SZAs especially in the tropics.

In Fig. 10, the formaldehyde slant columns for the whole cruise are shown. Different viewing angles (color coded) are separated clearly from each other except for periods with bad weather. For example, the low HCHO slant columns on 13 October are a consequence of heavy rain (wash out) in the morning (the formaldehyde slant columns recover after the strong rain but do not reach the level of other days' slant columns). The dominant peak on 20 October is the consequence of a light path extension in sea fog (the oxygen dimer O_4 shows a peak at the same time and the camera in our telescope housing shows a nebulous scene). Apart from this event, highest formaldehyde columns were obtained on 10 October (being in the polluted marine environment near Japan, compare Fig. 1c) and 24 October (approaching Ausralia's coast). Although the measurements were already stopped in the morning hours of 24 October when arriving in Townsville, Australia, a remarkable increase of formaldehyde slant columns was observed during the few hours of operation when approaching the coast, most likely connected to bush fires, as it was dry season and a lot of fires were observed in the next vicinity even by eye. 14 October (being on the open ocean, see Fig. 1) was the sunniest day of the cruise with best viewing conditions and lowest cloud coverage (around noon was the only completely cloud-free period throughout the cruise) going along with a local maximum in the HCHO timeseries. Thus, this maximum indicates that the observed formaldehyde results mainly from methane oxidation and subsequent HCHO production which depends on sunlight. A second local maximum in

ACPD
12, 15977–16024, 2012

the formaldehyde timeseries was found in the evening of 19 October, dominated by almost complete cloud coverage making a similar explanation as for the maximum on 14 October implausible. However, these measurements of enhanced formaldehyde were not performed on the open ocean, but close (≈150 km) to *New Ireland*[4] as shown in Fig. 12 (being a zoom-in of Fig. 1). In addition, 24-h-backward trajectories were calculated with the NOAA HYSPLIT model and displayed in green. The trajectories' starting point is in a distance of 10 km off the ship in the viewing direction of our instrument and in an altitude of 350 m a.s.l. as this was considered to be a reasonable approximation for the MAX-DOAS probed air at small elevation angles. The trajectories starting in the afternoon of 19 October reach back to the island groups of *Tabar* and *Lihir* after 12 h and to the island of *New Ireland* after less than 18 h. Backward trajectories starting in the evening of 19 October reach back to the island of *New Ireland* after ≈12 h (closest distance to the island ≈150 km in the evening of 19 October, which coincides with this day's HCHO maximum). Thus, the enhanced formaldehyde on 19 October, especially in the evening, is most probably a result of formaldehyde precursor transport from rainforest. On the next day, 20 October, Fig. 12 shows that the wind direction changed transporting clean air masses from the open sea to our position, resulting in lower formaldehyde slant columns.

Profiles and vertical columns of formaldehyde have been calculated using the profiling software BREAM (Sect. 3.5) consistent to the retrieval of tropospheric NO_2 (Sect. 4.2). Tropospheric HCHO columns were retrieved successfully during the whole cruise above an estimated detection limit of 0.5×10^{15} molec cm^{-2} (Fig. 13) and reproduce the local maxima as discussed above. In addition, the vertical columns exhibit

[4]New Ireland Province is part of the Bismarck Archipelago and the most northeastern province of Papua New Guinea encompassing the largest island of the province called *New Ireland* and numerous smaller islands including the *Tabar* and *Lihir group* at the Pacific side (the latter is famous for housing a gold mine holding one of the world's largest gold resources). The island of *New Ireland* has a length of ≈400 km but a width of mostly less than 10 km. The terrain is dominated by a central mountainous spine, the vegetation is tropical rainforest.

ACPD
12, 15977–16024, 2012

a diurnal cycle with low values in the morning and evening and maxima around noon, most clearly on days with good weather and viewing conditions, especially on 14 October.

As an example, Fig. 14 shows the retrieved profiles for 14 and 15 October, both having reasonable viewing conditions, although not being completely cloud-free. 14 October had the lowest cloud coverage throughout the whole cruise with a completely cloud-free period around noon when highest concentrations of 1.1 ppbv occured. In contrast, 15 October had its best viewing conditions (rarely cloudy) in the afternoon to evening, a partly to full cloud coverage in the morning and a short rain event at noon, most likely supressing a midday's maximum as seen on 14 October. The better viewing conditions on 14 October also result in a smoother shape of concentration isolines compared to 15 October. Both days show a diurnal cycle with enhanced levels of formaldehyde also in higher altitudes around noon when the sunlight intensity driving the formaldehyde production is highest. Corresponding peak concentrations of 1.1 ppbv in lower altitudes were found on 14 October at noon-time. In comparison to NO_2 showing highest concentrations close to the ground (see Fig. 9) formaldehyde's highest concentrations occur in an altitude of ≈400–600 m during the day and touch the surface in the morning and evening with slightly higher concentrations in the evening.

Judging from these results, cloud coverage seems to have a large influence on formaldehyde from methane oxidation making 14 October (and 15) the best examples for the (almost) cloud-free behaviour and developement of HCHO background concentration in the clean and remote marine environment. Reported concentrations from other studies range from 0.2–1.0 ppbv in remote marine environments (Singh et al., 2001; Weller et al., 2000) and therefore agree with our results although we found maximum concentrations of >1 ppbv in 400–600 m altitude under cloud-free conditions in the subtropical remote ocean (latitude ≈20° N) at noontime.

Due to the diurnal cycle found in formaldehyde vertical columns, care must be taken with respect to the comparison between MAX-DOAS and satellite measurements. Therefore, the vertical columns have been averaged between 9 and 11 local

ACPD
12, 15977–16024, 2012

time as this corresponds roughly to the satellite overflight time. In addition, as mentioned above, satellite instruments have a much shorter light path through the troposphere than MAX-DOAS instruments, resulting in a poorer sensitivity for tropospheric absorbers. Thus, as a result of the small amount of HCHO (pure background signal, see Fig. 11), the MAX-DOAS vertical columns had to be compared with monthly averages seen from satellite (Fig. 15). Due to the poor coverage of SCIAMACHY in comparison with GOME-2, this comparison could be performed only for GOME-2 data.

Two examples of the influence of bad weather can be found in the data (Fig. 15): the minimum of 1×10^{15} molec cm^{-2} at ≈24° N in MAX-DOAS data results from the low formaldehyde columns on 13 October (compare Fig. 13 and Fig. 10) which are a consequence of washing out. A second example is the delay of MAX-DOAS data in comparison to GOME-2 when increasing at ≈−10° S which is most likely an effect of comparing point-in-time measurements with monthly averages: as rainy and cloudy conditions predominated during the cruise in the coral sea (21–24 October, see Fig. 1), consequently, the MAX-DOAS measurements remain small, while GOME-2 values average also over periods with better weather and less clouds yielding higher formaldehyde concentrations.

As a consequence of the comparison of MAX-DOAS with monthly averages, the agreement of single maxima and minima cannot be expected. Apart from the effect of cloudy weather as discussed above, MAX-DOAS and GOME-2 data agree at a vertical column of about 3×10^{15} molec cm^{-2}, which can be considered as a typical value for the formaldehyde vertical column above the remote ocean for the time of the GOME-2 overflight.

5 Summary and conlusions

During the ship-borne field campaign TransBrom encountering polluted marine regions as well as clean open ocean conditions, formaldehyde and (stratospheric and tropospheric) nitrogen dioxide MAX-DOAS measurements were performed in the Western

ACPD
12, 15977–16024, 2012

Pacific. The objectives of this study were to retrieve background concentrations of these trace gases as well as validating measurements from the SCIAMACHY and GOME-2 satellite instruments.

For stratospheric NO_2, a characteristic latitude-dependant U-shaped behaviour was found, which is reproduced by both satellite instruments (Fig. 4). NO_2 morning values are lower than evening values due to slow photolysis of N_2O_5 during the course of the day. In low latitudes an increase of $8.7 \pm 0.5 \times 10^{13}$ molec cm^{-2} h^{-1} was found. The SCIAMACHY and GOME-2 NO_2 columns differ by only ≈1 % from each other and by a value of $(0.26–0.53) \pm 1.3 \times 10^{14}$ molec cm^{-2} from the MAX-DOAS morning values, which is a consequence of the satellite's overflight time (09:30 LT resp. 10:00 LT) and the stratospheric NO_2 diurnal cycle (Fig. 5).

Over the remote ocean, significantly enhanced columns of tropospheric NO_2 were found only in regions, where higher ship traffic could be verified (i.e. crossing of shipping routes, see Fig. 6 and 1c). In the polluted marine environment close to Japan, NO_2 events were observed with peak concentrations up to 0.8 ppbv close to the ground whereas the background concentration did not exceed 0.2 ppbv. When leaving the region influenced by the Japanese islands and the anthropogenic activities (shipping) connected to it, the tropospheric NO_2 columns decreased below an estimated detection limit of 1.3×10^{14} molec cm^{-2} (50 pptv) (see Fig. 8), which can therefore be considered to be an upper estimate for the tropospheric NO_2 column in the clean air over the remote ocean. This estimated background concentration is lower than model values suggesting ≈4×10^{14} molec cm^{-2} for the tropospheric NO_2 column above the Pacific ocean between 180°–210° longitude (Hilboll et al., 2012). Close to the Japanese coast, averages of vertical columns from the satellite instruments are 2–3 times higher than corresponding MAX-DOAS vertical columns as a consequence of enhanced levels of NO_2 over Japan. Over the remote ocean, the monthly average column from GOME-2 is in good agreement with the estimated NO_2 background column derived from MAX-DOAS data (see above).

ACPD
12, 15977–16024, 2012

Profiles and vertical columns of formaldehyde (Fig. 13) originating from methane oxidation show a characteristic diurnal cycle over the tropical and subtropical ocean (most apparent on almost cloud-free days) with maxima at noon in an altitude of 400–600 m (Fig. 14). This background formaldehyde concentration was found to be highly dependent on the cloud coverage while no latitudinal dependence in the region 40° N to −20° S could be observed (Figs. 13 and 15). Maximum values for the vertical column on cloud-free occasions were found to be $\approx 4 \times 10^{15}$ molec cm^{-2} corresponding to a peak concentration of 1.1 ppbv (Figs. 13 and 14), which is sligtly higher than earlier reported values ranging from 0.2–1 ppbv (Weller et al., 2000; Singh et al., 2001; Burkert et al., 2001). In addition, a transport event of formaldehyde (or it's precursors) was found ≈150 km away from the only possible source (island with rainforest vegetation) and calculated backward trajectories suggest that the formaldehyde or it's precursors bridged this distance in 12–18 h before being detected by our MAX-DOAS instrument. The GOME-2 and MAX-DOAS measurements agree on typical values of $\approx 3 \times 10^{15}$ molec cm^{-2} for the remote ocean at the overpass time.

Acknowledgements. We acknowledge the GEOMAR in Kiel, Germany, especially Kirstin Krüger and Birgit Quack for organizing the national WGL project TransBrom and the TransBrom-SONNE (BMBF) ship campaign. The ship measurements work for this paper were partly funded by the BMBF through grant 03G0731A. The contribution from University of Bremen was supported by the EU via the GEOMon Integrated Project (contract FP6-2005-Global-4-036677). The Bremen instrument was partly funded by the University of Bremen and the ENVIVAL-life project (50EE0839). Douglas Horton and his team from US Coast Guard Operations Systems Center provided ship position data from the Automated Mutual-Assistance Vessel Rescue System (AMVER). Backward trajectories were calculated with the HYSPLIT online tool from the National Oceanic and Atmospheric Administration (NOAA). For his helpful comments, many thanks also to Klaus Pfeilsticker from IUP Heidelberg.

ACPD
12, 15977–16024, 2012

References

Anderson, L. G., Lanning, J. A., Barrell, R., Miyagishima, J., Jones, R. H., and Wolfe, P.: Sources and sinks of formaldehyde and acetaldehyde: an analysis of Denver's ambient concentration data, Atmos. Environ., 30, 2113–2123, 1996. 15980

Arlander, D. W., Brüning, D., Schmidt, U., and Ehhalt, D. H.: The tropospheric distribution of formaldehyde during TROPOZ II, J. Atmos. Chem., 22, 251–268, 1995. 15980

Bates, D. R. and Hays, P. B.: Atmospheric nitrous oxide, Planet. Space Sci., 15, 189–197, 1967. 15979

Beirle, S., Platt, U., von Glasow, R., Wenig, M., and Wagner, T.: Estimate of nitrogen oxide emissions from shipping by satellite remote sensing, Geophys. Res. Lett., 31, L18102, doi:10.1029/2004GL020312, 2004. 15993

Boersma, K. F., Eskes, H. J., and Brinksma, E. J.: Error analysis for tropospheric NO_2 retrieval from space, J. Geophys. Res., 109, D04311, doi:10.1029/2003JD003962, 2004. 15995

Bogumil, K., Orphal, J., Homann, T., Voigt, S., Spietz, P., Fleischmann, O. C., Vogel, A., Hartmann, M., Kromminga, H., Bovensmann, H., Frerick, J., and Burrows, J. P.: Measurements of molecular absorption spectra with the SCIAMACHY pre-flight model: instrument characterization and reference data for atmospheric remote-sensing in the 230–2380 nm region, J. Photochem. Photobiol. A, 157, 167–184, 2003. 15987

Bovensmann, H., Burrows, J. P., Buchwitz, M., Frerick, J., Noël, S., Rozanov, V. V., Chance, K. V., and Goede, A. P. H.: SCIAMACHY: mission objectives and measurement modes, J. Atmos. Sci., 56, 127–150, 1999. 15984

Brasseur, G. P., Orlando, J. J., and Tyndall, G. S.: Atmospheric Chemistry and Global Change, Oxford University Press, New York, 1999. 15979, 15989

Burkert, J., Andres-Hernandez, M. D., Stobener, D., Burrows, J. P., Weissenmayer, M., and Kraus, A.: Peroxy radical and related trace gas measurements in the boundary layer above the Atlantic Ocean, J. Geophys. Res.-Atmos., 106, 5457–5477, 2001. 15980, 16001

Burrows, J. P., Hölzle, E., Goede, A. P. H., Visser, H., and Fricke, W.: SCIAMACHY – scanning imaging absorption spectrometer for atmospheric chartography, Acta Astronaut., 35, 445–451, 1995. 15984

Burrows, J. P., Weber, M., Buchwitz, M., Rozanov, V., Ladstatter-Weissenmayer, A., Richter, A., DeBeek, R., Hoogen, R., Bramstedt, K., Eichmann, K. U., and Eisinger, M.: The global ozone

ACPD
12, 15977–16024, 2012

monitoring experiment (GOME): mission concept and first scientific results, J. Atmos. Sci., 56, 151–175, 1999. 15984

Callies, J., Corpaccioli, E., Eisinger, M., Hahne, A., and Lefebvre, A.: GOME-2 – Metop's second-generation sensor for operational ozone monitoring, Esa Bull.-Eur. Space, 102, 28–36, 2000. 15984

Crutzen, P. J.: The influence of nitrogen oxides on the atmospheric ozone content, Q. J. Roy. Meteor. Soc., 96, 320–325, 1970. 15979

De Smedt, I., Müller, J.-F., Stavrakou, T., van der A, R., Eskes, H., and Van Roozendael, M.: Twelve years of global observations of formaldehyde in the troposphere using GOME and SCIAMACHY sensors, Atmos. Chem. Phys., 8, 4947–4963, doi:10.5194/acp-8-4947-2008, 2008. 15980

Draxler, R. R. and Rolph, G. D.: HYSPLIT (HYbrid Single-Particle Lagrangian Integrated Trajectory) model access via NOAA ARL READY website, available at: http://ready.arl.noaa.gov/HYSPLIT.php (last access: September 2011), 2011. 15981, 15994

Fleischmann, O. C., Hartmann, M., Burrows, J. P., and Orphal, J.: New ultraviolet absorption cross-sections of BrO at atmospheric temperatures measured by time-windowing Fourier transform spectroscopy, J. Photochem. Photobiol. A, 168, 117–132, 2004. 15987

Franke, K., Richter, A., Bovensmann, H., Eyring, V., Jöckel, P., Hoor, P., and Burrows, J. P.: Ship emitted NO_2 in the Indian Ocean: comparison of model results with satellite data, Atmos. Chem. Phys., 9, 7289–7301, doi:10.5194/acp-9-7289-2009, 2009. 15979

Frieß, U., Sihler, H., Sander, R., Pöhler, D., Yilmaz, S., and Platt, U.: The vertical distribution of BrO and aerosols in the Arctic: measurements by active and passive differential optical absorption spectroscopy, J. Geophys. Res., 116, D00R04, doi:10.1029/2011JD015938, 2011. 15988

Gil, M., Yela, M., Gunn, L. N., Richter, A., Alonso, I., Chipperfield, M. P., Cuevas, E., Iglesias, J., Navarro, M., Puentedura, O., and Rodríguez, S.: NO_2 climatology in the northern subtropical region: diurnal, seasonal and interannual variability, Atmos. Chem. Phys., 8, 1635–1648, doi:10.5194/acp-8-1635-2008, 2008. 15989

Großmann, K., Frieß, U., Tschritter, J., Peters, E., Wittrock, F., Quack, B., Krüger, K., Sommariva, R., Glasow, R. V., Pfeilsticker, K., and Platt, U.: Iodine monoxide in the Western Pacific marine boundary layer, Atmos. Chem. Phys. Discuss., in preparation, 2012. 15987

ACPD
12, 15977–16024, 2012

Heckel, A., Richter, A., Tarsu, T., Wittrock, F., Hak, C., Pundt, I., Junkermann, W., and Burrows, J. P.: MAX-DOAS measurements of formaldehyde in the Po-Valley, Atmos. Chem. Phys., 5, 909–918, doi:10.5194/acp-5-909-2005, 2005. 15987

Hilboll, A., Richter, A., Rozanov, A., Hodnebrog, Ø, Heckel, A., Solberg, S., Stordal, F., and Burrows, J. P.: Retrieval of tropospheric NO_2 columns from SCIAMACHY combining measurements from limb and nadir geometries, Atmos. Meas. Tech. Discuss., in preparation, 2012. 16000

Hönninger, G., von Friedeburg, C., and Platt, U.: Multi axis differential optical absorption spectroscopy (MAX-DOAS), Atmos. Chem. Phys., 4, 231–254, doi:10.5194/acp-4-231-2004, 2004. 15983

Irie, H., Kanaya, Y., Akimoto, H., Tanimoto, H., Wang, Z., Gleason, J. F., and Bucsela, E. J.: Validation of OMI tropospheric NO_2 column data using MAX-DOAS measurements deep inside the North China Plain in June 2006: Mount Tai Experiment 2006, Atmos. Chem. Phys., 8, 6577–6586, doi:10.5194/acp-8-6577-2008, 2008. 15980

Johnston, H.: Reduction of stratospheric ozone by nitrogen oxide catalysts from supersonic transport exhaust, Science, 173, 517–522, 1971. 15979

Konovalov, I. B., Beekmann, M., Richter, A., Burrows, J. P., and Hilboll, A.: Multi-annual changes of NO_x emissions in megacity regions: nonlinear trend analysis of satellite measurement based estimates, Atmos. Chem. Phys., 10, 8481–8498, doi:10.5194/acp-10-8481-2010, 2010. 15979

Kreher, K., Fiedler, M., Gomer, T., Stutz, J., and Platt, U.: The latitudinal distribution (50° N–50° S) of NO_2 and O_3 in October/November 1990, Geophys. Res. Lett., 22, 1217–1220, 1995. 15991

Krüger, K. and Quack, B.: Introduction to special issue: the *TransBrom Sonne* expedition in the tropical West Pacific, Atmos. Chem. Phys. Discuss., 12, 1401–1418, doi:10.5194/acpd-12-1401-2012, 2012. 15981

Lee, D. S., Köhler, I., Grobler, E., Rohrer, F., Sausen, R., Gallardo-Klenner, L., Olivier, J. G. J., Dentener, F. J., and Bouwman, A. F.: Estimations of global NO_x emissions and their uncertainties, Atmos. Environ., 31, 1735–1749, 1997. 15979

Leue, C., Wenig, M., Wagner, T., Klimm, O., Platt, U., and Jahne, B.: Quantitative analysis of NO_x emissions from global Ozone Monitoring Experiment satellite image sequences, J. Geophys. Res.-Atmos., 106, 5493–5505, 2001. 15980

ACPD
12, 15977–16024, 2012

Marbach, T., Beirle, S., Platt, U., Hoor, P., Wittrock, F., Richter, A., Vrekoussis, M., Grzegorski, M., Burrows, J. P., and Wagner, T.: Satellite measurements of formaldehyde linked to shipping emissions, Atmos. Chem. Phys., 9, 8223–8234, doi:10.5194/acp-9-8223-2009, 2009. 15980

Martin, M., Pöhler, D., Seitz, K., Sinreich, R., and Platt, U.: BrO measurements over the Eastern North-Atlantic, Atmos. Chem. Phys., 9, 9545–9554, doi:10.5194/acp-9-9545-2009, 2009. 15980

Martin, R. V., Chance, K., Jacob, D. J., Kurosu, T. P., Spurr, R. J. D., Bucsela, E., Gleason, J. F., Palmer, P. I., Bey, I., Fiore, A. M., Li, Q. B., Yantosca, R. M., and Koelemeijer, R. B. A.: An improved retrieval of tropospheric nitrogen dioxide from GOME, J. Geophys. Res.-Atmos., 107, 4437, doi:10.1029/2001JD001027, 2002. 15980

Meller, R. and Moortgat, G. K.: Temperature dependence of the absorption cross sections of formaldehyde between 223 and 323 K in the wavelength range 225–375 nm, J. Geophys. Res., 105, 7089–7101, 2000. 15987

Palmer, P. I., Jacob, D. J., Fiore, A. M., Martin, R. V., Chance, K., and Kurosu, T. P.: Mapping isoprene emissions over North America using formaldehyde column observations from space, J. Geophys. Res.-Atmos., 108, 4180, doi:10.1029/2002JD002153, 2003. 15980

Pinardi, G., Roozendael, M. V., Adams, C., Beirle, S., Cede, A., Clémer, K., Fayt, C., Friess, U., Gil, M., Hermans, C., Hendrick, F., Irie, H., Merlaud, A., Peters, E., Piters, A., Puentedura, O., Richter, A., Shaigan, R., Spinei, E., Strong, K., Takashima, H., Wagner, T., Wittrock, F., and Yilmaz, S.: Intercomparison of MAXDOAS formaldehyde slant column measurements during the CINDI campaign, Atmos. Meas. Tech. Discuss., in preparation, 2012. 15986, 15987

Piters, A. J. M., Boersma, K. F., Kroon, M., Hains, J. C., Van Roozendael, M., Wittrock, F., Abuhassan, N., Adams, C., Akrami, M., Allaart, M. A. F., Apituley, A., Beirle, S., Bergwerff, J. B., Berkhout, A. J. C., Brunner, D., Cede, A., Chong, J., Clémer, K., Fayt, C., Frieß, U., Gast, L. F. L., Gil-Ojeda, M., Goutail, F., Graves, R., Griesfeller, A., Großmann, K., Hemerijckx, G., Hendrick, F., Henzing, B., Herman, J., Hermans, C., Hoexum, M., van der Hoff, G. R., Irie, H., Johnston, P. V., Kanaya, Y., Kim, Y. J., Klein Baltink, H., Kreher, K., de Leeuw, G., Leigh, R., Merlaud, A., Moerman, M. M., Monks, P. S., Mount, G. H., Navarro-Comas, M., Oetjen, H., Pazmino, A., Perez-Camacho, M., Peters, E., du Piesanie, A., Pinardi, G., Puentedura, O., Richter, A., Roscoe, H. K., Schönhardt, A., Schwarzenbach, B., Shaiganfar, R., Sluis, W., Spinei, E., Stolk, A. P., Strong, K., Swart, D. P. J., Takashima, H., Vlemmix, T., Vrekoussis, M., Wagner, T., Whyte, C., Wilson, K. M., Yela, M., Yilmaz, S., Zieger, P.,

ACPD
12, 15977–16024, 2012

and Zhou, Y.: The Cabauw Intercomparison campaign for Nitrogen Dioxide measuring Instruments (CINDI): design, execution, and early results, Atmos. Meas. Tech., 5, 457–485, doi:10.5194/amt-5-457-2012, 2012. 15986
Platt, U.: Differential optical absorption spectroscopy (DOAS), Chem. Anal. Series, 127, 27–83, 1994. 15980
Platt, U. and Stutz, J.: Differential Optical Absorption Spectroscopy: Principles and Applications, Physics of Earth and Space Environments, Springer Verlag, Berlin Heidelberg, 2008. 15983
Quack, B.: Cruise Report TransBrom SONNE, Tech. rep., IFM Geomar, Kiel, Germany, 2010. 15981
Raymond, C. and Baker, K. S.: Optical properties of the clearest natural waters, Appl. Optics, 20, 177–184, 1981. 15987
Richter, A.: Absorptionsspektroskopische Messungen stratosphärischer Spurengase über Bremen, 53°N, Ph.D. thesis, University of Bremen, Bremen, Germany, 1997. 15987
Richter, A. and Burrows, J. P.: Tropospheric NO_2 frome GOME Measurements, Adv. Space Res., 29, 1673–1683, 2002. 15979
Richter, A., Eyring, V., Burrows, J. P., Bovensmann, H., Lauer, A., Sierk, B., and Crutzen, P. J.: Satellite measurements of NO_2 from international shipping emissions, Geophys. Res. Lett., 31, L23110, doi:10.1029/2004GL020822, 2004. 15979, 15980, 15993
Richter, A., Burrows, J. P., Nüß, H., Granier, C., and Niemeier, U.: Increase in tropospheric nitrogen dioxide over China observed from space, Nature, 437, 129–132, 2005. 15980, 15989
Richter, A., Begoin, M., Hilboll, A., and Burrows, J. P.: An improved NO_2 retrieval for the GOME-2 satellite instrument, Atmos. Meas. Tech., 4, 1147–1159, doi:10.5194/amt-4-1147-2011, 2011. 15989
Rodgers, C. D.: Inverse Methods for Atmospheric Sounding – Theory and Practice, Series on Atmospheric, Oceanic and Planetary Physics, World Scientific, Singapore, 2000. 15988
Rolph, G. D.: Real-time Environmental Applications and Display sYstem (READY) Website, available at: http://ready.arl.noaa.gov (last access: September 2011), 2011. 15981, 15994
Roscoe, H. K., Van Roozendael, M., Fayt, C., du Piesanie, A., Abuhassan, N., Adams, C., Akrami, M., Cede, A., Chong, J., Clémer, K., Friess, U., Gil Ojeda, M., Goutail, F., Graves, R., Griesfeller, A., Grossmann, K., Hemerijckx, G., Hendrick, F., Herman, J., Hermans, C., Irie, H., Johnston, P. V., Kanaya, Y., Kreher, K., Leigh, R., Merlaud, A., Mount, G. H., Navarro, M., Oetjen, H., Pazmino, A., Perez-Camacho, M., Peters, E., Pinardi, G., Puent-

ACPD
12, 15977–16024, 2012

edura, O., Richter, A., Schönhardt, A., Shaiganfar, R., Spinei, E., Strong, K., Takashima, H., Vlemmix, T., Vrekoussis, M., Wagner, T., Wittrock, F., Yela, M., Yilmaz, S., Boersma, F., Hains, J., Kroon, M., Piters, A., and Kim, Y. J.: Intercomparison of slant column measurements of NO_2 and O_4 by MAX-DOAS and zenith-sky UV and visible spectrometers, Atmos. Meas. Tech., 3, 1629–1646, doi:10.5194/amt-3-1629-2010, 2010. 15986

Rozanov, A., Rozanov, V., Buchwitz, M., Kokhanovsky, A., and Burrows, J. P.: SCIATRAN 2.0 – a new radiative transfer model for geophysical applications in the 175–2400 nm spectral region, Adv. Space Res., 36, 1015–1019, 2005. 15987

Seco, R., Peñuelas, J., and Filella, I.: Short-chain oxygenated VOCs: emission and uptake by plants and atmospheric sources, sinks, and concentrations, Atmos. Environ., 41, 2477–2499, 2006. 15980

Singh, H., Chen, Y., Staudt, A., Jacob, D., Blake, D., Heikes, B., and Snow, J.: Evidence from the Pacific troposphere for large global sources of oxygenated organic compounds, Nature, 410, 1078–1081, 2001. 15980, 15998, 16001

Sinreich, R., Coburn, S., Dix, B., and Volkamer, R.: Ship-based detection of glyoxal over the remote tropical Pacific Ocean, Atmos. Chem. Phys., 10, 11359–11371, doi:10.5194/acp-10-11359-2010, 2010. 15980

Stavrakou, T., Müller, J.-F., De Smedt, I., Van Roozendael, M., van der Werf, G. R., Giglio, L., and Guenther, A.: Global emissions of non-methane hydrocarbons deduced from SCIAMACHY formaldehyde columns through 2003–2006, Atmos. Chem. Phys., 9, 3663–3679, doi:10.5194/acp-9-3663-2009, 2009. 15980

Takashima, H., Irie, H., Kanaya, Y., and Syamsudin, F.: NO_2 observations over the Western Pacific and Indian Ocean by MAX-DOAS on Kaiyo, a Japanese research vessel, Atmos. Meas. Tech. Discuss., 4, 6069–6095, doi:10.5194/amtd-4-6069-2011, 2011. 15980, 15992, 15995

Vandaele, A. C., Hermans, C., Simon, P. C., Roozendael, M. V., Guilmot, J. M., Carleer, M., and Colin, R.: Fourier transform measurement of NO_2 absorption cross-section in the visible range at room temperature, J. Atmos. Chem., 25, 289–305, 1996. 15987

Vountas, M., Rozanov, V. V., and Burrows, J. P.: Ring effect: impact of rotational Raman scattering on radiative transfer in Earth's atmosphere, J. Quant. Spectrosc. Ra., 60, 943–961, 1998. 15987

ACPD
12, 15977–16024, 2012

Vountas, M., Richter, A., Wittrock, F., and Burrows, J. P.: Inelastic scattering in ocean water and its impact on trace gas retrievals from satellite data, Atmos. Chem. Phys., 3, 1365–1375, doi:10.5194/acp-3-1365-2003, 2003. 15980

Vrekoussis, M., Wittrock, F., Richter, A., and Burrows, J. P.: GOME-2 observations of oxygenated VOCs: what can we learn from the ratio glyoxal to formaldehyde on a global scale?, Atmos. Chem. Phys., 10, 10145–10160, doi:10.5194/acp-10-10145-2010, 2010. 15989

Wagner, T., Beirle, S., Brauers, T., Deutschmann, T., Frieß, U., Hak, C., Halla, J. D., Heue, K. P., Junkermann, W., Li, X., Platt, U., and Pundt-Gruber, I.: Inversion of tropospheric profiles of aerosol extinction and HCHO and NO_2 mixing ratios from MAX-DOAS observations in Milano during the summer of 2003 and comparison with independent data sets, Atmos. Meas. Tech., 4, 2685–2715, doi:10.5194/amt-4-2685-2011, 2011. 15988

Wang, P., Stammes, P., van der A, R., Pinardi, G., and van Roozendael, M.: FRESCO+: an improved O_2 A-band cloud retrieval algorithm for tropospheric trace gas retrievals, Atmos. Chem. Phys., 8, 6565–6576, doi:10.5194/acp-8-6565-2008, 2008. 15989

Weller, R., Schrems, O., Boddenberg, A., Gäb, S., and Gautrois, M.: Meridional distribution of hydroperoxides and formaldehyde in the marine boundary layer of the Atlantic (48° N–35° S) measured during the Albatross campaign, J. Geophys. Res., 105, 14401–14412, 2000. 15980, 15998, 16001

Wittrock, F.: The retrieval of oxygenated volatile organic compounds by remote sensing techniques, available at: http://www.doas-bremen.de/paper/diss_wittrock_06.pdf (last access: April 2012), Ph.D., University of Bremen, Bremen, Germany, 2006. 15988

Wittrock, F., Richter, A., Ladstätter-Weißenmayer, A., and Burrows, J. P.: Global Observations of Formaldehyde, Proceedings of the ERS-ENVISAT Symposium, ESA Publication SP-461, ESRIN, the ESA centre for Earth Observation, in Frascati, 2000. 15980

Wittrock, F., Oetjen, H., Richter, A., Fietkau, S., Medeke, T., Rozanov, A., and Burrows, J. P.: MAX-DOAS measurements of atmospheric trace gases in Ny-Ålesund – Radiative transfer studies and their application, Atmos. Chem. Phys., 4, 955–966, doi:10.5194/acp-4-955-2004, 2004. 15983

Wittrock, F., Richter, A., Oetjen, H., Burrows, J. P., Kanakidou, M., Myriokefalitakis, S., Volkamer, R., Beirle, S., Platt, U., and Wagner, T.: Simultaneous global observations of glyoxal and formaldehyde from space, Geophys. Res. Lett., 33, L16804, doi:10.1029/2006GL026310, 2006. 15980

ACPD

12, 15977–16024, 2012

Wittrock, F., Clémer, K., Beirle, S., Berkhout, S., Brunner, D., Friess, U., Hay, T., Irie, H., Kreher, K., Oetjen, H., Peters, E., Piters, A., Richter, A., Van Roozendael, M., Sluis, W., Spinei, E., and Wagner, T.: Measurements of NO_2 profiles with MAX-DOAS: Theoretical and practical case studies as part of the Cabauw Intercomparison campaign for Nitrogen Dioxide Measuring Instruments (CINDI), Atmos. Meas. Tech. Discuss., in preparation, 2012. 15988

ACPD
12, 15977–16024, 2012

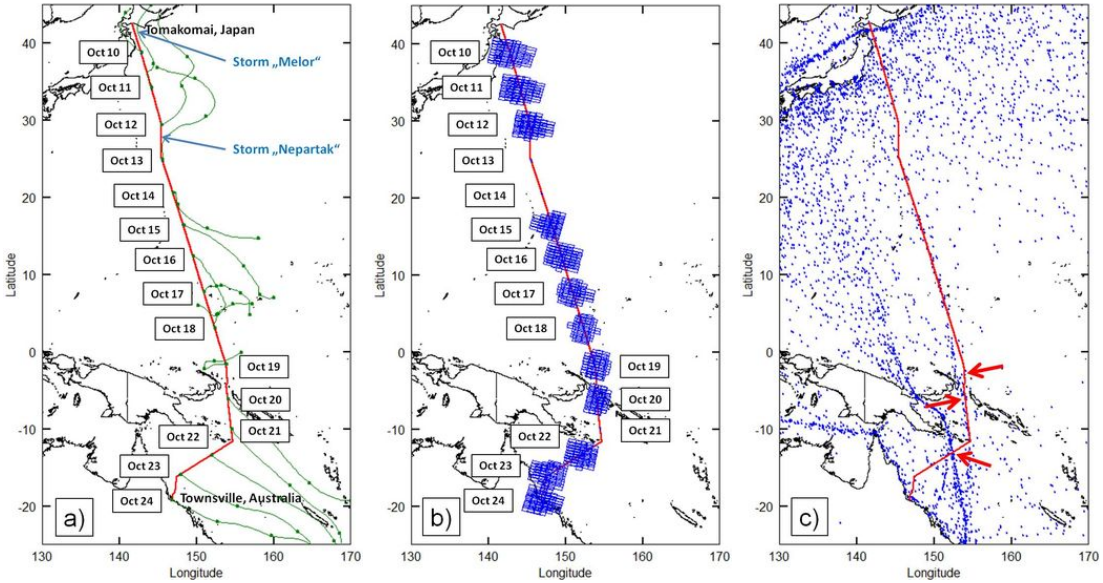

Fig. 1. (a) TransBrom Cruise Track (red) and 72 h backward trajectories calculated by the NOAA HYSPLIT model (green marks indicate starting point, −1 day, −2 days, −3 days). **(b)** GOME-2 satellite pixels within a radius of 200 km around the ship's positions at the time of the overflight. **(c)** Ship density for 10–24 October 2009 (ship positions reported to the US Coast Guard AMVER System).

ACPD
12, 15977–16024, 2012

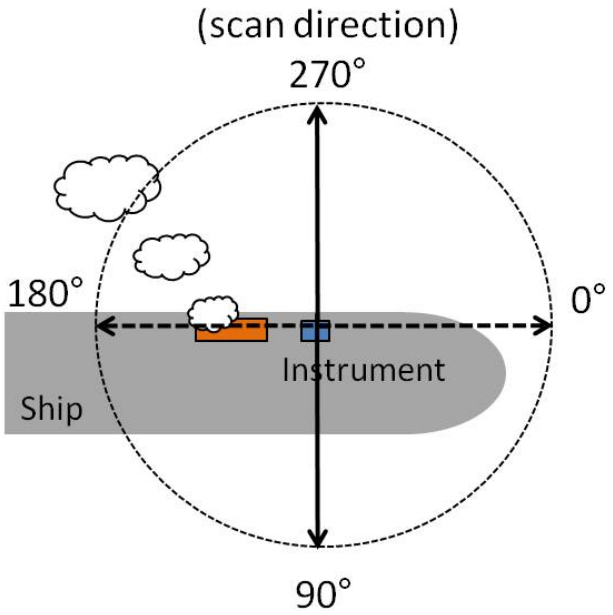

Fig. 2. Schematic bird's eye view of the vessel. Vertical scans were performed in the 270° direction (rectangular to ship's movement). Relative wind directions between 90° and 270° were excluded as our ship's plume would contaminate the zenith pointing reference spectra and/or the vertical scans.

ACPD
12, 15977–16024, 2012

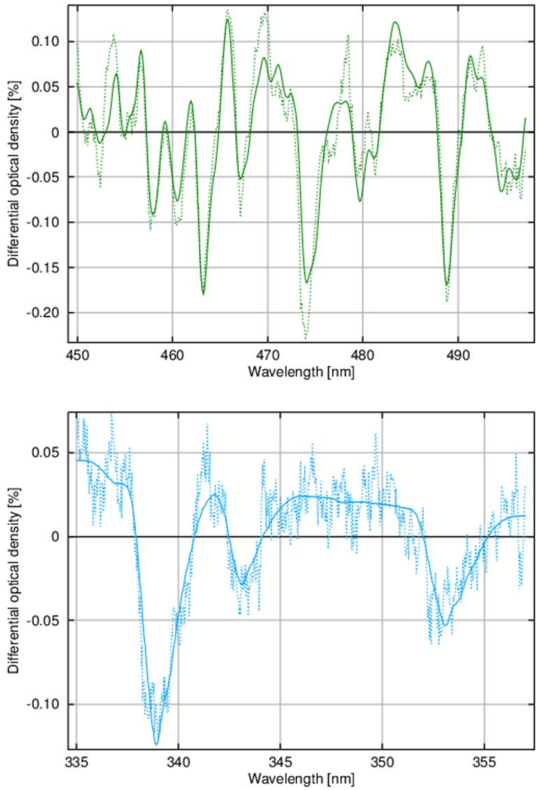

Fig. 3. Example fits for tropospheric NO_2 in green (slant column 1.38×10^{16} molec cm^{-2}, RMS 2.8×10^{-4}) and HCHO in blue (slant column 2.82×10^{16} molec cm^{-2}, RMS 1.6×10^{-4}) from 10 October 2009 (03:24 UT, 47.6° SZA, 2° viewing angle). The solid line is the scaled cross-section (with the scaling factor being the slant column) and the dashed line is the fit (scaled cross-section plus fit residual).

ACPD
12, 15977–16024, 2012

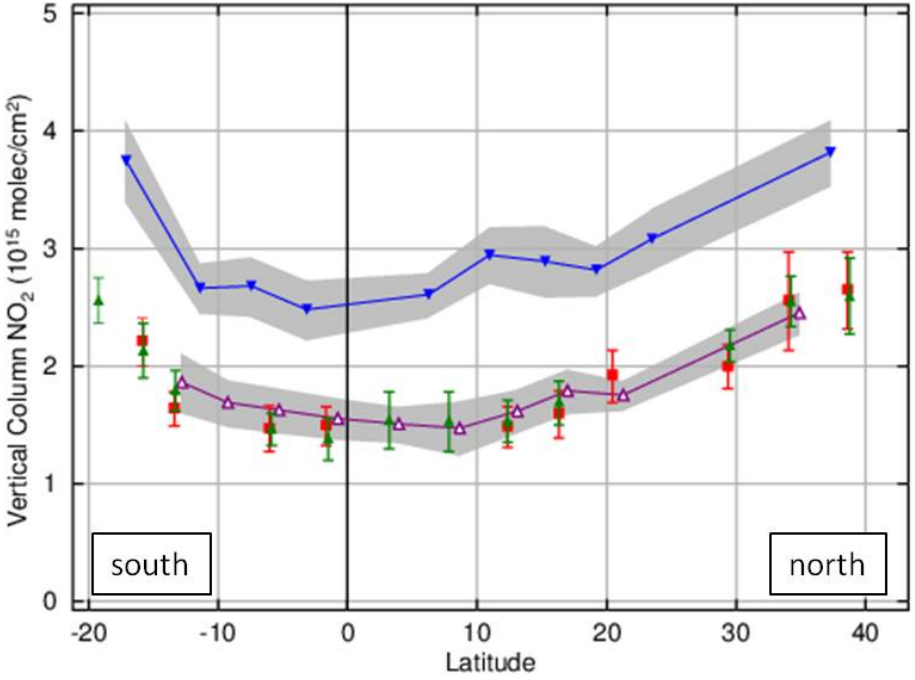

Fig. 4. Stratospheric NO_2 vertical columns as a function of latitude, MAX-DOAS morning values in magenta, evening values in blue (gray-shaded area indicates error margin), GOME-2 satellite values are displayed in green, SCIAMACHY satellite values in red (see text).

ACPD
12, 15977–16024, 2012

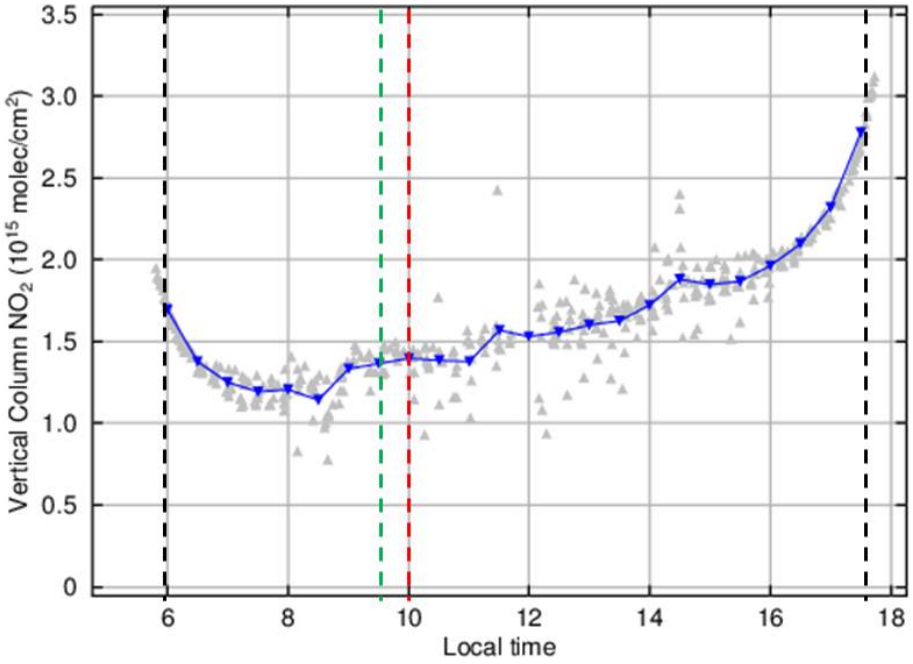

Fig. 5. Diurnal cycle of stratospheric NO_2 vertical columns on 15 October 2009 (grey: single measurements, blue: data binned to 0.5 h resolution). The black dashed lines give the positions of 90° SZA in the morning and evening, the green dashed line gives the approximate GOME-2 overpass time and the red dashed line the SCIAMACHY overpass.

ACPD
12, 15977–16024, 2012

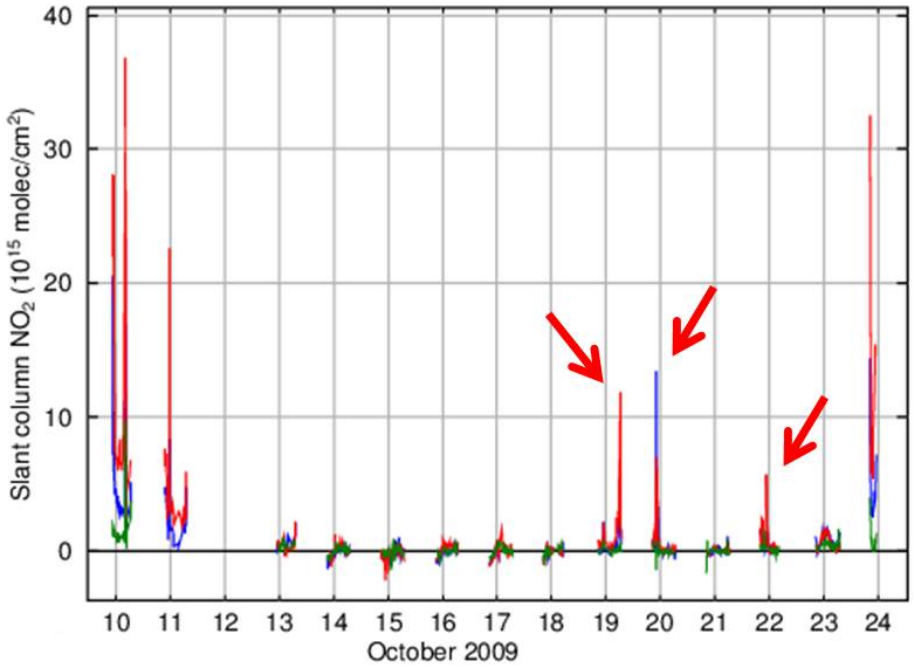

Fig. 6. Color-coded tropospheric NO_2 slant columns (red = 2°, blue = 8°, green = 30°) using closest zenith reference spectra; for 11 October spectra at 30° elevation angle have been used as reference due to instrumental problems. Measurements taken at *bad* wind directions (e.g. 12 October) have been removed preventing contamination from the ship's plume. Except for the first two days (influence from Japan) and when approaching Australia's coast (last day), NO_2 columns over the open ocean were above the detection limit (2×10^{15} molec cm^{-2}, see text) only during three events (red arrows corresponding to the ship's position indicated by arrows in Fig. 1c).

ACPD
12, 15977–16024, 2012

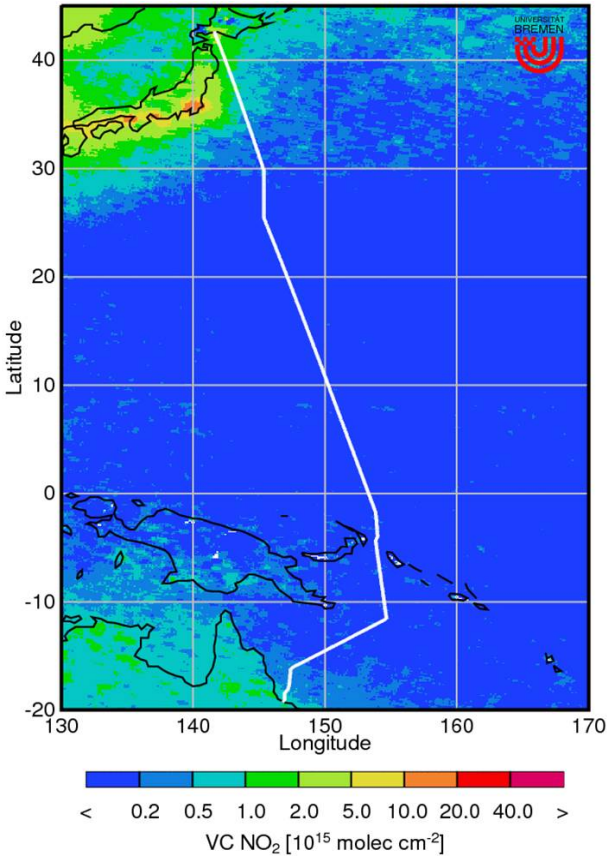

Fig. 7. October 2009 monthly average of tropospheric NO_2 from GOME-2 (scientific product from Institute of Environmental Physics, University of Bremen). The Cruise Track is indicated. After the first days, having influences from Japan, a region of pure NO_2 background concentration is encountered.

ACPD
12, 15977–16024, 2012

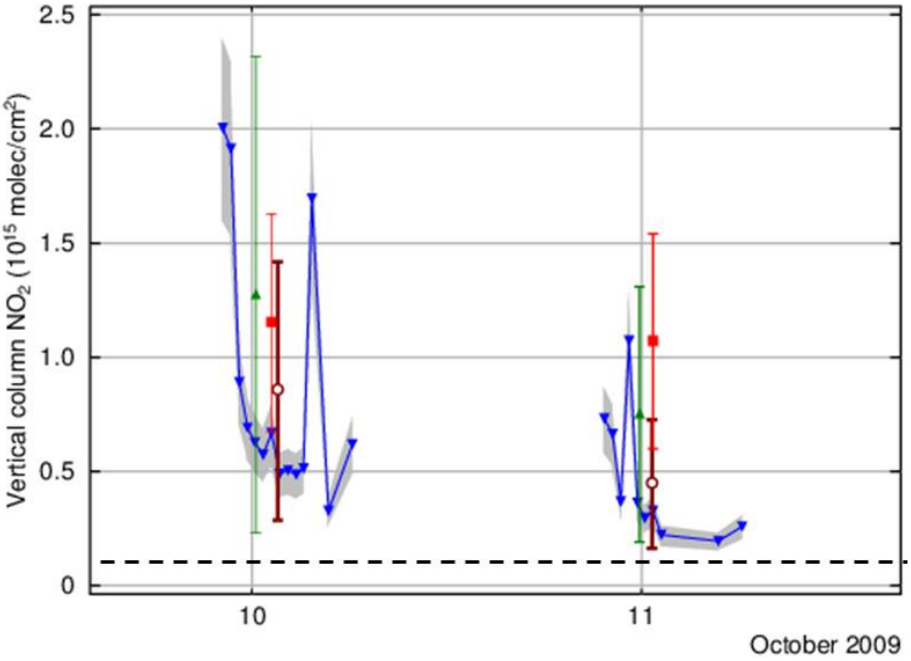

Fig. 8. Retrieved vertical NO_2 columns from MAX-DOAS measurements for 10 and 11 October 2009 in blue, GOME-2 values in green (satellite pixels averaged within 150 km around ship's position at time of overflight) and SCIAMACHY values in red (200 km radius). The dashed line indicates the MAX-DOAS detection limit. Brown: MAX-DOAS averages (see text).

ACPD
12, 15977–16024, 2012

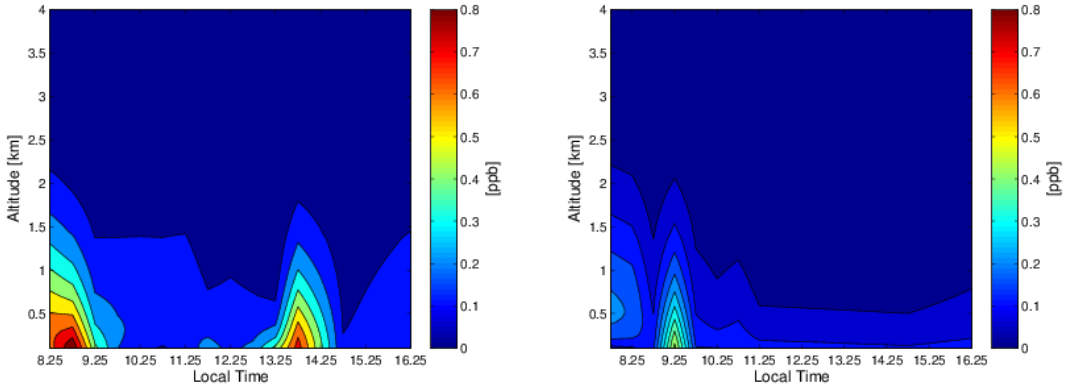

Fig. 9. Retrieved NO_2 profiles for 10 October (left) and 11 October (right). Highest NO_2 concentrations are close to the ground. The maxima on 10 October result most likely from influences from Japan while the peak on 11 October is another ship's plume.

ACPD
12, 15977–16024, 2012

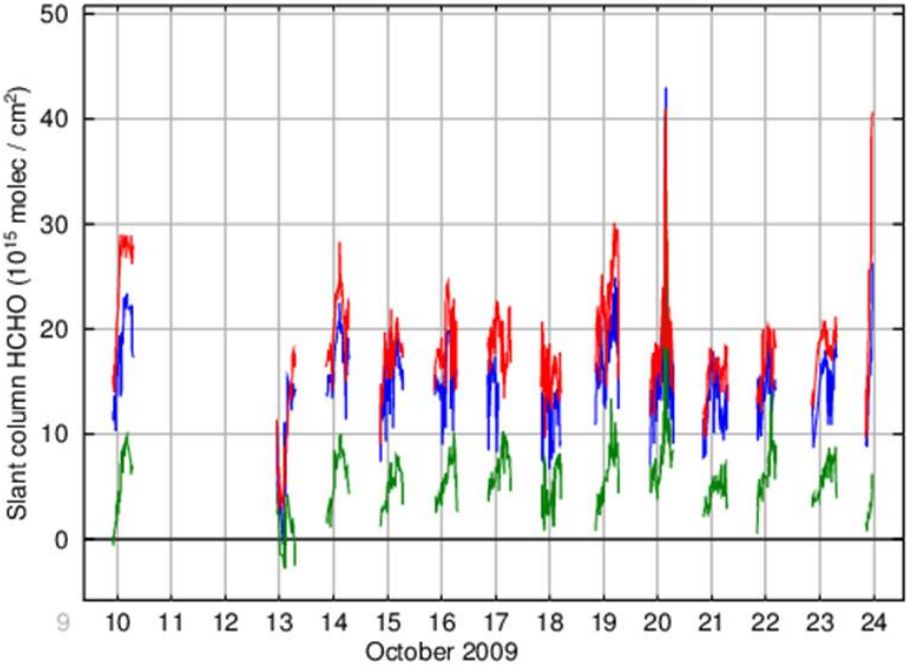

Fig. 10. Color-coded formaldehyde slant columns (red = 2°, blue = 8°, green = 30°). Different viewing directions split-up well for the whole campaign indicating a background level of HCHO in the marine boundary layer. No data is shown for 11 and 12 October due to a lack of zenith measurements (used as reference, see text) on 11 October and *bad* wind directions on 12 October.

ACPD
12, 15977–16024, 2012

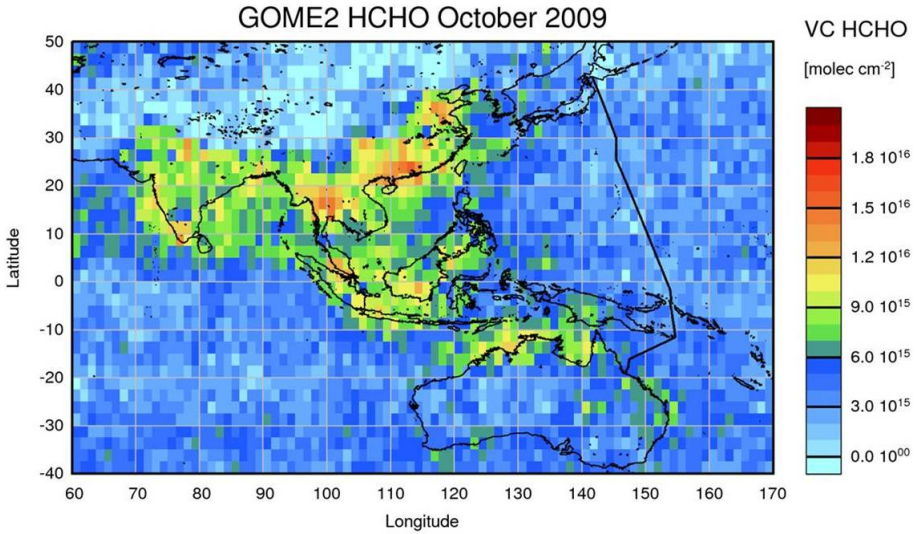

Fig. 11. October 2009 monthly average of tropospheric formaldehyde from the GOME-2 instrument (scientific product from Institute of Environmental Physics, University of Bremen). Measured HCHO columns during TransBrom (the cruise track is indicated) are background concentrations from methane oxidation (possible anthropogenic contributions at the beginning and end of the cruise).

ACPD
12, 15977–16024, 2012

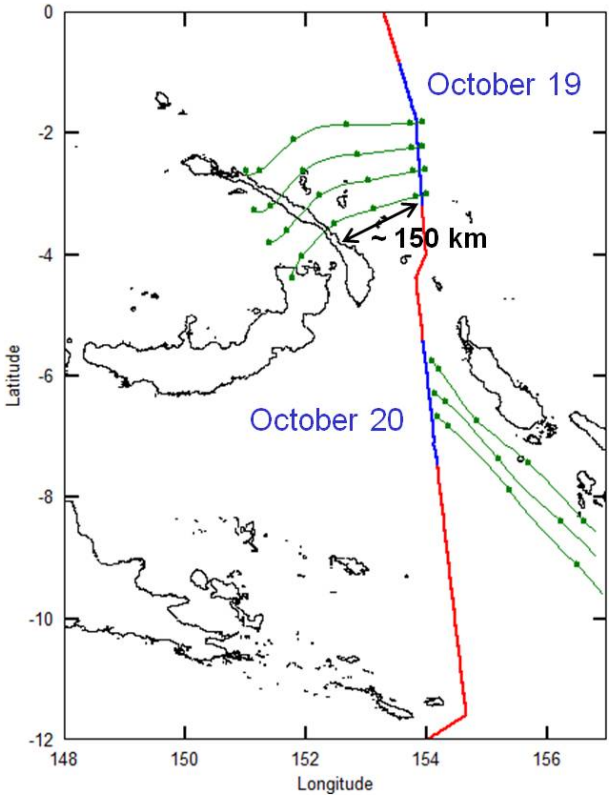

Fig. 12. Detail map of the TransBrom cruise. Blue parts indicate 19 and 20 October daytime, when MAX-DOAS measurements were performed. Backward trajectories are displayed in green, marks meaning: starting point, −1, −6, −12, −18 and −24 h, respectively.

ACPD
12, 15977–16024, 2012

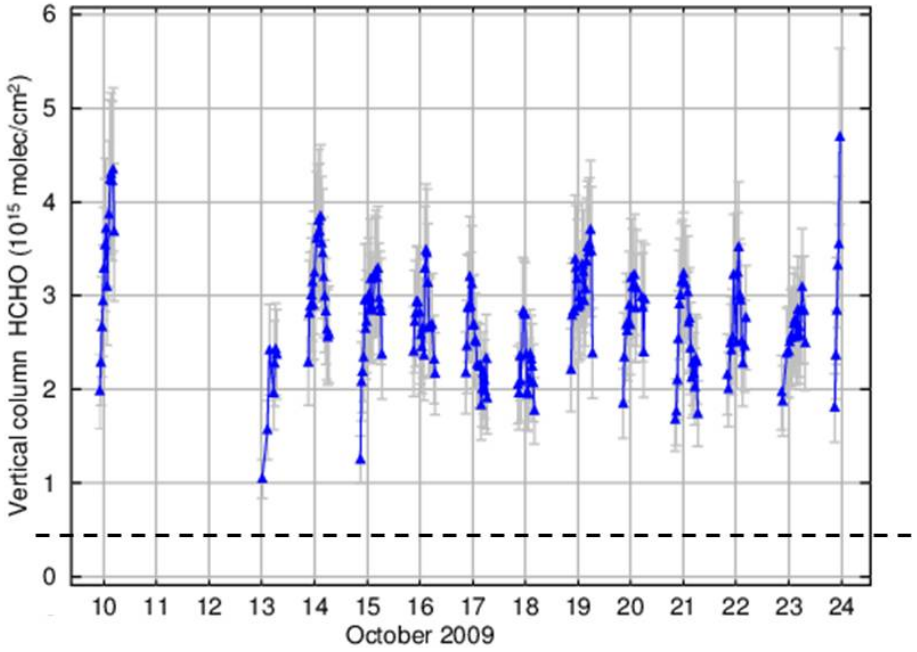

Fig. 13. Time series of the retrieved tropospheric HCHO vertical columns. The dashed line indicates the MAX-DOAS detection limit.

ACPD
12, 15977–16024, 2012

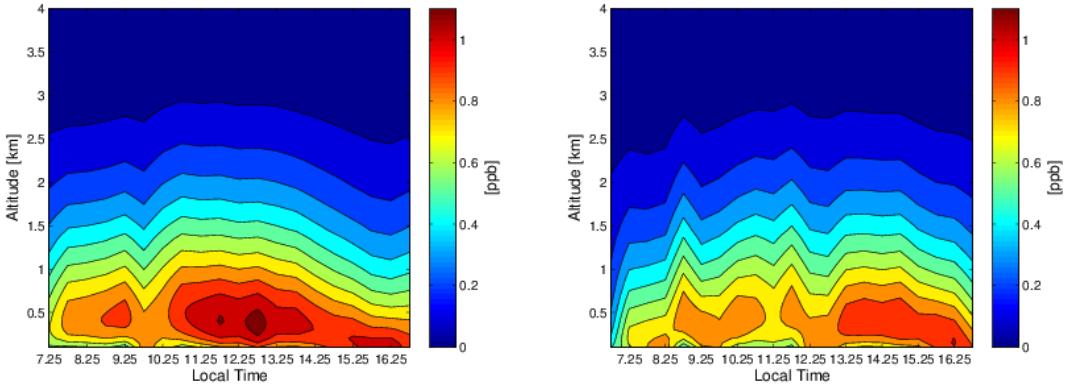

Fig. 14. Retrieved formaldehyde profiles for 14 October (left) and 15 October (right) having reasonable viewing conditions. The only completely cloud-free period of the cruise was on 14 October around noon coinciding with maximum formaldehyde concentrations of 1.1 ppbv in an altitude of ≈400 m.

ACPD
12, 15977–16024, 2012

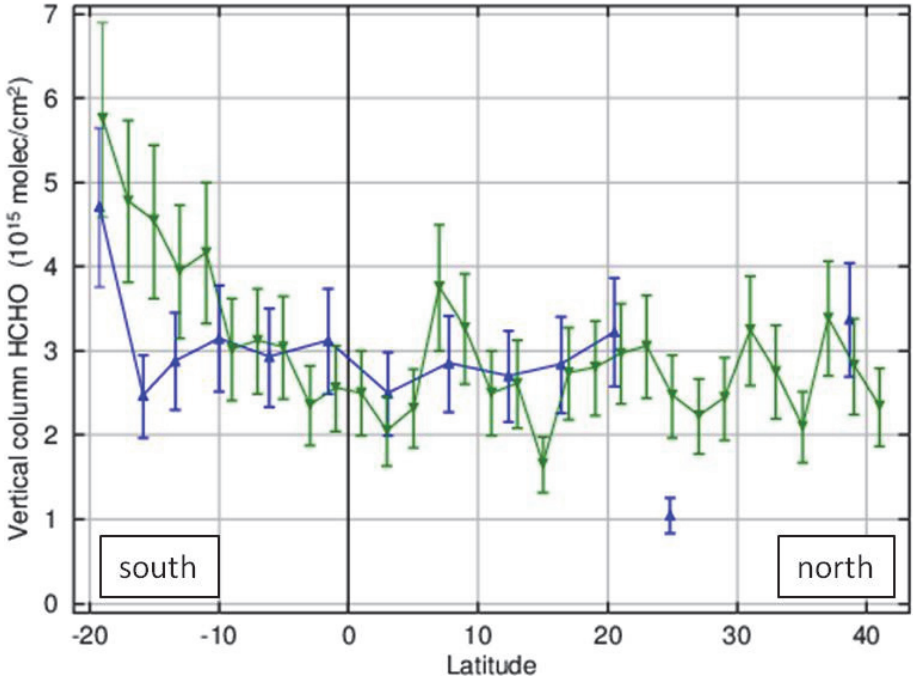

Fig. 15. Comparison between MAX-DOAS (blue) and GOME-2 (green) HCHO vertical columns as a function of latitude. MAX-DOAS data was averaged between 09:00–11:00 LT (approx. time of GOME-2 overflight). The GOME-2 values are calculated from monthly average for October 2009 and binned to a 2° grid for better visualisation of the results.

ACPD
12, 15977–16024, 2012